Morphology and Properties of Nanocomposites Formed from Poly(ethylene-*co*-methacrylic acid) Ionomers and Organoclays: Effect of Acid Neutralization

Lili Cui,[†] Christina Troeltzsch,[‡] P. J. Yoon,[§] and D. R. Paul*,[†]

Department of Chemical Engineering and Texas Materials Institute, The University of Texas at Austin, Austin, Texas 78712; E. I. DuPont Company, Sabine River Works, P.O. Box 1089, Orange, Texas 77631; and Southern Clay Products, 1212 Church Street, Gonzales, Texas 78629

Received January 17, 2009; Revised Manuscript Received February 19, 2009

ABSTRACT: Nanocomposites were prepared by melt blending a series of sodium ionomers formed from poly(ethylene-*co*-methacrylic acid) and the $M_2(HT)_2$ organoclay. The effects of the degree of neutralization of the acid groups on the morphology and properties of the nanocomposites were evaluated using stress−strain analysis, wide-angle X-ray scattering (WAXS), and transmission electron microscopy coupled with particle analysis. The organoclay exfoliation improves progressively as the neutralization level of the sodium ionomers increases. It seems that the ionic units on polymer chains provide a more favorable interaction between the polymer matrix and organoclay than acid units. Predictions of the tensile modulus of the nanocomposites by the Halpin−Tsai equations capture some of the experimental trends, but the absolute values do not agree well with the experimental observations.

Introduction

Nanocomposites formed by melt blending polymers with an organically modified clay mineral montmorillonite (MMT) have attracted a great deal of interest in the past decade. Numerous studies have demonstrated that the addition of only a few percent of this layered silicate can lead to significant property enhancements over the polymer matrix, e.g., increased stiffness and strength,[1−3] lower linear coefficient of thermal expansion,[4,5] enhanced gas barrier properties,[6−8] and superior flame retardancy.[9−11] However, to take advantage of the high aspect ratio of these nanometer thick silicate platelets, as compared to conventional reinforcing fillers, requires achieving high levels of exfoliation of the clay. Although optimizing the processing conditions is helpful in organoclay exfoliation, the favorable interaction between polymer matrix and organoclay is the key to high levels of exfoliation in nanocomposites.

For nonpolar polyolefins, uniform dispersion and effective exfoliation are particularly difficult to achieve due to the poor affinity of the polymer matrix for the hydrophilic silicate platelets. Considerable effort has been devoted to improving the exfoliation in these materials. Use of compatibilizers, such as maleated polypropylene or maleated polyethylene, is one of the popular choices.[12−16] Incorporation of polar comonomers like vinyl acetate[17−19] or methacrylic acid[20−23] is another attractive approach. Ionomers, such as those based on poly(ethylene-*co*-methacrylic acid) (EMAA), where some of the acid groups are neutralized to form metal salts, represent an extension of this approach. The presence of the ionic groups potentially creates favorable interactions between the polymer and the organoclay, resulting in a more exfoliated morphology.

Various structural aspects of an ionomer matrix could have an effect on its ability to exfoliate the organoclays, such as molecular weight (melt index), acid content, type of acid, type of neutralizing ion, and degree of neutralization. Previous studies by Shah et al. focused on the effect of different cations[24] and finding the best organoclay structure for a given sodium ionomer.[25]

This study explores the effect of the degree of neutralization of the acid groups on exfoliation and properties of nanocomposites formed from such materials. These nanocomposites were characterized by tensile stress−strain tests, Izod impact measurements, wide-angle X-ray scattering (WAXS), and transmission electron microscopy (TEM) coupled with quantitative particle analysis.

Experimental Section

Materials. The experimental ionomers shown in Table 1were based on an EMAA copolymer containing 15 wt % of methacrylic acid. The series of materials are sodium ionomers with neutralization levels ranging from 20% to 70%. These materials were prepared by DuPont by extrusion neutralization of an etheylene−methacrylic acid base resin. A commercial grade of EMAA copolymer (Nucrel 925, 15 wt % acid content) was included as an unneutralized reference material. It should be noted that this acid copolymer is not the base resin used to form the ionomer materials but is a higher molecular weight version in an attempt to keep the melt rheology more comparable to that of the ionomers.

The $M_2(HT)_2$ organoclay, formed by cationic exchange between sodium montmorillonite (CEC = 92 mequiv/100 g clay) and dimethyl bis(hydrogenated-tallow) quaternary ammonium salt, was from Southern Clay Products, Inc. Some frequently used abbreviations[17,26] are employed here to represent the substituents on the ammonium cation, e.g., M for methyl and HT represents long alkyl chains from hydrogenated tallow. Several other organoclays were explored as part of this study; however, in the intent of brevity, these results are not included here but are available elsewhere.[27] The best exfoliation was always found for nanocomposites based on the $M_2(HT)_2$ organoclay, which is consistent with a prior report[25] from this laboratory using a commercial grade of EMAA ionomer with ∼40% neutralization of the acid groups.

Processing. Ionomer nanocomposites were prepared by melt compounding in a Haake, corotating, intermeshing twin-screw extruder (D = 30 mm, L/D = 10) at a screw speed of 280 rpm with a feed rate of 1000 g/h, using a barrel temperature in the range of 200−220 °C depending on the degree of neutralization of the ionomer. Ionomers and acid copolymer materials were dried in a vacuum oven for a minimum of 48 h prior to the compounding, while the organoclays were used as received. The data below are reported in terms of the weight percent montmorillonite (MMT) in

* Corresponding author: Tel 512-471-5392; fax 512-471-0542, e-mail drp@che.utexas.edu.
[†] The University of Texas at Austin.
[‡] E. I. DuPont Company.
[§] Southern Clay Products.

10.1021/ma900105w CCC: $40.75
Published on Web 03/10/2009

Table 1. Polymers Used in This Study

polymers		type of counterion	acid content (wt %)	melt index (g/10 min)	neutralization (%)	ion (wt %)
EMAA	Nucrel 925		15	25	0	0
ionomer 1	experimental	Na	15	47.7	20	0.80
ionomer 2	experimental	Na	15	24.9	30	1.20
ionomer 3	experimental	Na	15	12.6	40	1.60
ionomer 4	experimental	Na	15	5.93	50	2.00
ionomer 5	experimental	Na	15	2.29	60	2.40
ionomer 6	experimental	Na	15	0.98	70	2.74

the composites rather than the amount of organoclay, since the silicate is the reinforcing component. The desired amounts of clay and polymer were premixed before feeding to the extruder, and precautions were taken to minimize any losses of organoclay during the extrusion process to ensure that a predetermined polymer/MMT ratio was maintained. The ashing method, commonly used in prior studies from this laboratory[28−31] to determine the amount of montmorillonite in the nanocomposite, was not employed for these ionomers, since the burning of the polymer itself at 900 °C resulted in a hard, yellowish-green coating on the inside of the crucible reflecting some complex residue of the inorganic component of the ionomer. The amount of the residue varied from sample to sample, rendering this method useless for quantitative analysis.

Tensile (ASTM D638) and Izod (ASTM D256) specimens were formed using an Arburg Allrounder 305-210-700 injection molding machine operated at a barrel temperature of 210 °C and a mold temperature of 25 °C, with the injection and holding pressures both set at 40 bar. After molding, the specimens were immediately sealed in a polyethylene bag and placed in a vacuum desiccator for a minimum of 24 h prior to mechanical testing.

Characterization. Dynamic rheological measurements were performed using a Stresstech high-resolution rheometer. Rheological properties of virgin ionomers were measured using 25 mm diameter parallel plates in an oscillatory shear mode. Complex viscosity was obtained as a function of angular frequency at 200 °C. The frequency sweep was over the range from 0.01 to 100 rad/s. A fixed strain of 0.02 was used to ensure that measurements were taken within the linear viscoelastic range. Experiments were conducted under a nitrogen atmosphere in order to minimize oxidative degradation of the specimens during testing.

Differential scanning calorimetric (DSC) thermograms were recorded using a Perkin-Elmer Model DSC-7 at a heating rate of 10 °C/min under an extra dry N_2 atmosphere over a temperature range of 0−140 °C. The predried virgin ionomer samples weighing about 8 mg were packed in aluminum pans, melted, and then kept in a desiccator for 2 weeks before the measurements. These pretreatments were conducted to remove previous thermal history, and each sample experienced the same length of room temperature aging time, since a number of factors, such as moisture content and room temperature aging, can affect the details of the DSC thermograms.[32−34]

X-ray diffraction scans were obtained using a Bruker-AXS D8 Advance diffractometer in the reflection mode with an incident X-ray wavelength of 1.541 Å, at a scan rate of 3.0°/min over the range of 1°−12°. Scans were performed on organoclay powder and injection-molded nanocomposites (Izod bars); the bars were orientated such that the incident beam reflected off the plane comprised of the transverse and flow direction.[35]

Ultrathin sections (∼50 nm) were cut with a diamond knife from the central part of the Izod bars in the plane parallel to the flow direction under cryogenic conditions using an RMC PowerTome XL microtome. These sections were collected on 400 mesh copper grids and subsequently dried with filter paper. TEM images were obtained using a JEOL 2010F transmission electron microscope operating at an accelerating voltage of 120 kV. A subsequent quantitative particle analysis of these images was conducted to determine the particle length, thickness, and various averages of the aspect ratio using similar methods described in prior papers.[17,30]

Tensile tests were performed at room temperature according to ASTM D696 on an Instron model 1137 machine upgraded for computerized data acquisition. Modulus values were determined using an extensometer at a crosshead speed of 0.51 cm/min. Elongation at break was measured at a crosshead speed of 5.1 cm/min. Yield stress data are not reported because the stress−strain diagrams of some of the nanocomposites do not show a distinct yield point. Notched Izod impact tests were performed at room temperature using a TMI Izod tester (6.8 J hammer and 3.5 m/s impact velocity) according to ASTM D 256. As common practice, Izod bars were cut in half to generate more samples. Since significant differences are shown between the two ends of the bars, data are reported as separately averaged values for far-end and gate-end specimens. Data reported here represent an average from measurements on at least five specimens.

Properties of Neat Ionomers

Before discussing the morphology and properties of the nanocomposites, it is useful to examine the properties of the neat ionomers.

Melt Viscosity. Ideally, materials with similar melt viscosities should be selected to compare the effect of matrix chemical structure on organoclay exfoliation, since the melt rheology may affect organoclay exfoliation in polymer nanocomposites;[36] however, since the degree of neutralization has a strong effect on melt rheology, there is no simple way to produce a series of ionomers like those of interest here with similar melt viscosities. Oscillatory rheological measurements were performed at 200 °C on three partially neutralized sodium ionomers with neutralization levels of 30%, 50%, and 70% over an angular frequency from 0.01 to 100 rad/s (see Figure 1). As expected, all the polymers show Newtonian behavior at low frequency, while at higher frequencies the complex viscosity begins to decrease or show shear thinning. The melt viscosity increases dramatically as the neutralization level of the acid groups in the ionomer is increased; the low shear viscosity increased by more than 1 order of magnitude as the neutralization of the methacrylic acid groups increased from 30% to 70%. These results are consistent with the observations from previous reports.[32,37−39] At the high shear rates used in melt processing,

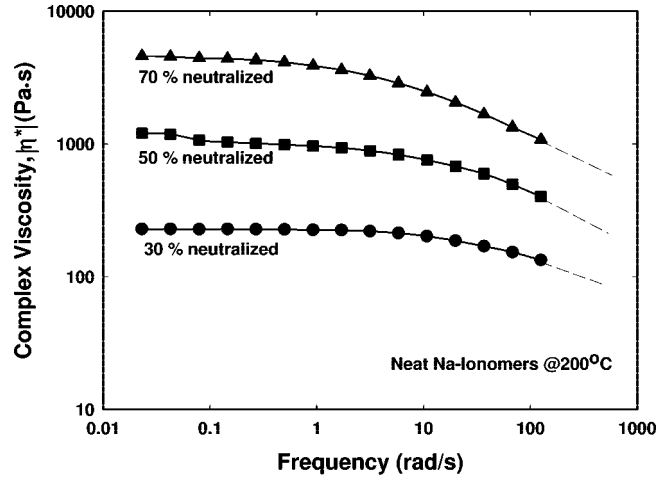

Figure 1. Complex viscosity for selected neat sodium ionomers with various neutralization levels as a function of frequency measured with a parallel plate rheometer at 200 °C.

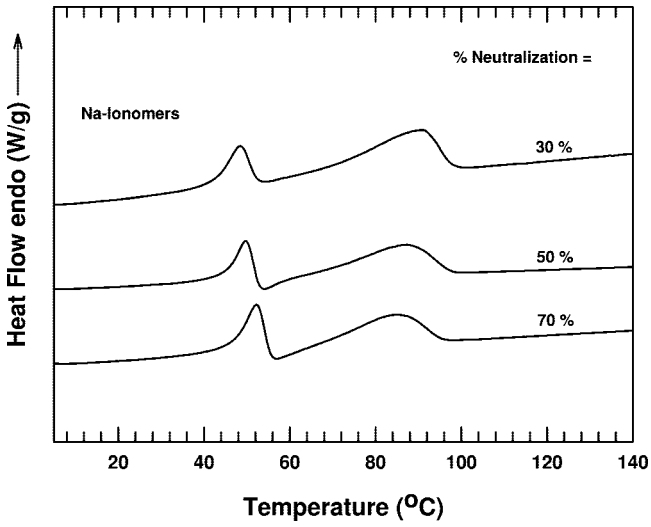

Figure 2. DSC thermograms of selected neat ionomers with various neutralization levels at 10 °C/min. The curves are vertically shifted for clarity.

Table 2. DSC Results for Neat Ionomer Polymers

sample	neutralization level (%)	T_i (°C)	ΔH_i (J/g)	T_m (°C)	ΔH_m (J/g)
ionomer 2	30	48.4	12.8	90.5	40.2
ionomer 4	50	49.7	16.0	86.5	37.2
ionomer 6	70	52.2	19.9	83.8	32.0

the effect of degree of neutralization on melt viscosity is not as great as the data in Figure 1 would suggest; however, this effect should not be ignored. To compensate for this, in part, the extrusion temperature was adjusted to keep the energy input to the mixing process, as indicated by the power consumption by the extruder, as close to constant as possible. That is, as the degree of neutralization increased, the extrusion temperature was increased. However, the effects of neutralization on melt viscosity, during melt processing, cannot be completely compensated in this way.

Differential Scanning Calorimetry (DSC). These ionomer materials have a complex morphology because of the aggregation of the ionic groups superimposed on the crystallinity stemming from ethylene sequences. The DSC scans shown in Figure 2 provide some insights about the structure of these materials.

Each of the three ionomers in Figure 2 shows two distinctive endothermic peaks. The one near 87 °C corresponds to the melting of crystallites formed from ethylene sequences (T_m). The low-temperature peak (T_i) near 50 °C was first reported by Marx and Cooper,[40] and several interpretations have been offered[40−45] since then. Currently there is not complete agreement on the details of this peak; some believe it is associated with changes in the state of ionic aggregation, while others attribute it to the melting of secondary crystallites.

The peak temperatures and the enthalpy changes associated with each peak are shown in Table 2. As the degree of neutralization increases, the T_m and the melting enthalpy (ΔH_m) decrease, while T_i and the associated heat (ΔH_i) increase. These trends seem reasonable considering that increasing neutralization levels would lead to greater ionic association and introduce more restrictions to crystallization of the ethylene sequences.

Mechanical Properties. The mechanical properties of the neat polymers are plotted versus the degree of neutralization in Figure 3. The data points for the acid copolymer are connected with those of the sodium ionomers using dashed lines because this copolymer is not the base resin used to form the ionomers.

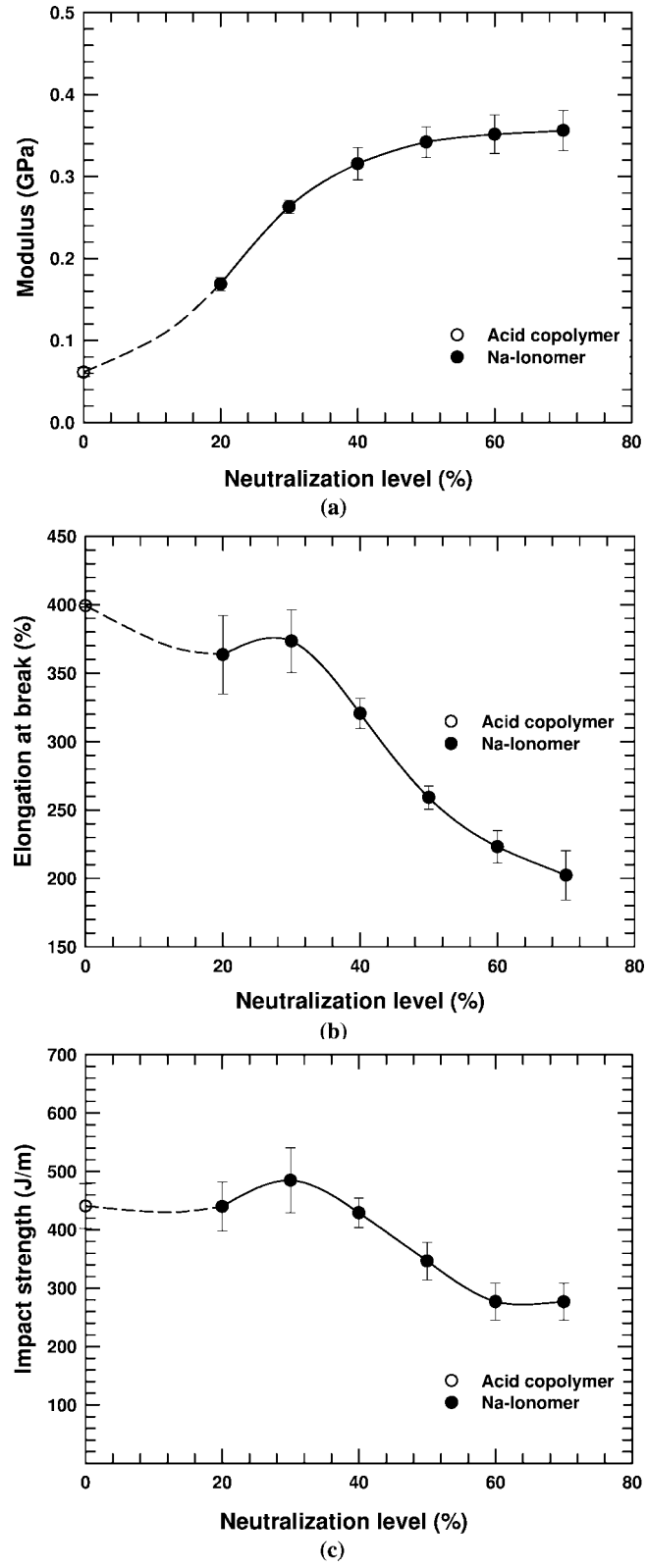

Figure 3. Effect of neutralization level on mechanical properties of neat polymers used in this study: (a) tensile modulus, (b) elongation at break, and (c) impact strength.

The tensile modulus (Figure 3a) increases significantly as the level of neutralization of acid groups increases, but the curve appears to plateau as the neutralization level reaches 40%. These trends are consistent with those reported previously.[32,39,46] The increase in modulus may be attributed to the increased volume of ionic aggregates that act as a reinforcing filler and increase

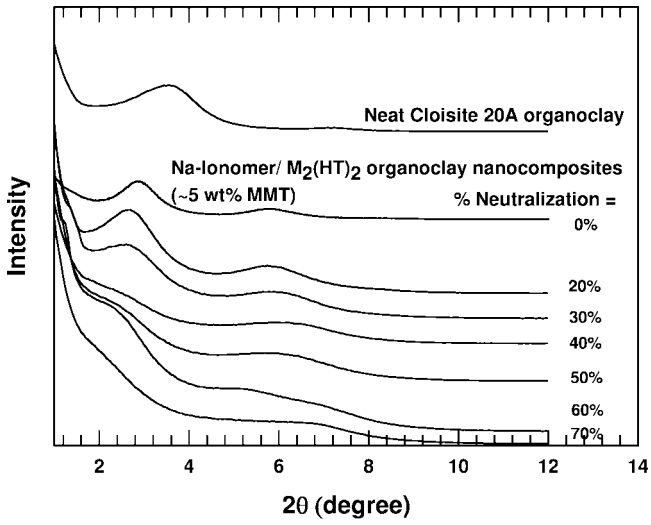

Figure 4. WAXS scans for the pristine $M_2(HT)_2$ organoclay and nanocomposites containing ~5 wt % MMT formed from sodium ionomers with various neutralization levels. The curves are vertically shifted for clarity.

Table 3. Comparison of *d*-Spacings for Various Nanocomposites[a]

polymer matrix	organoclay	*d*-spacing (d_{001}, nm)
	$M_2(HT)_2$	2.42[b]
EMAA		3.13
ionomer 1		3.34
ionomer 2		3.40
ionomer 3		
ionomer 4		
ionomer 5		
ionomer 6		

[a] Nanocomposites for WAXS study all contain nominally 5 wt % MMT. [b] *d*-spacings here represent that of the neat organoclay.

the glass transition temperature.[38,47−49] On the other hand, the elongation at break generally decreases with increasing neutralization levels as shown in Figure 3b. It is not clear whether the apparent minimum/maximum at low degrees of neutralization suggested by these data is significant or not. However, the impact strength of the neat polymers (see Figure 3c) seems to mimic the trends in the elongation at break data to some extent. The impact strength initially increases with neutralization, reaches a maximum at 30% neutralization, then decreases with further neutralization, and may increase again.

Nanocomposites

Morphology. WAXS scans of nanocomposites containing ~5 wt % MMT formed from the EMAA copolymer and the sodium ionomers are shown in Figure 4; a scan for the neat $M_2(HT)_2$ organoclay is also included for comparison. The *d*-spacings calculated from the d_{001} peak positions are summarized in Table 3. The scan for the neat organoclay reveals an intense peak around $2\theta = 3.6°$, which is characteristic of the basal spacing of the modified layered silicate. The nanocomposites based on ionomers with low neutralization levels (0−30%) show distinctive peaks that are shifted to lower angles compared to the organoclay itself; traditionally, this is attributed to the intercalation of polymer into the clay galleries. For nanocomposites based on ionomers with higher neutralization levels, no obvious peak was observed; however, there are slight hints of curvature at lower angles as compared to the peak position of the neat organoclay. These results suggest that the organoclay exfoliation improves with the increased neutralization level of the acid groups in ionomers. It should be noted that the WAXS patterns in Figure 4 show only one basal reflection for the organoclays, while higher order reflections were also observed for the nanocomposite samples. The organoclay scans were made from powders while the nanocomposite scans were performed on injection-molded samples. The high degree of orientation of clay platelets in the latter lead to multiple reflections, while the more random orientation in the organoclay powders do not.[50]

Properly prepared TEM images offer direct visualization of the dispersion of the clay particles in nanocomposites. Figure 5 compares TEM images of nanocomposites formed from the $M_2(HT)_2$ organoclay and sodium ionomers with various degrees of neutralization; the montmorillonite content in all cases is nominally 5 wt %. Morphologies consisting of combinations of individual platelets and intercalated stacks of platelets are observed for all the nanocomposites, indicating good, but not complete, exfoliation of the organoclays. It appears that the particles are smaller and more numerous in nanocomposites based on ionomers with higher degrees of neutralization of the acid groups; for the ionomer that is 70% neutralized, the organoclay exfoliation is significantly improved as compared to nanocomposites from EMAA copolymer and other sodium ionomers with lower neutralization levels. It appears that the ionic units promote exfoliation of the organoclay.

As mentioned earlier, one may argue that the increase in melt viscosity with increasing neutralization levels may also contribute to the better organoclay exfoliation. However, a close comparison of nanocomposites based on the ionomer with 30% neutralization clearly shows that it has much better exfoliation than nanocomposites based on the unneutralized EMAA copolymer, and these two polymers have very similar melt index values. Of course, the melt processing was done at much higher shear rates than used in the melt index measurement; however, because the molecular weight distributions are similar for the two materials, their melt viscosities will approach each other as shear rate is increased but the curves should never intersect. Thus, the high shear viscosities should stand in the same relationship as indicated by the melt indices but even closer in value. Thus, it seems that there is a beneficial effect of ionic groups for facilitating organoclay exfoliation as suggested in prior work.[20,24,25]

For a quantitative and more convincing assessment of the level of organoclay exfoliation, detailed particle analyses were conducted on the TEM images using methods introduced in prior papers.[17,30] For the best statistical reliability, a large number of particles (>400) were analyzed for each nanocomposite; the particle dimensions can be averaged in different ways. The statistical results of the particle analyses for nanocomposites containing 5 wt % MMT are listed in Table 4. As reported previously,[17,51,52] the aspect ratios calculated by averaging the values for each particle, $\langle l/t\rangle_n$ and $\langle l/t\rangle_w$, are always larger than those calculated from the ratio of the corresponding average particle length and average particle thickness, i.e., $\bar{l}_n/\bar{t}_n$ and $\bar{l}_w/\bar{t}_w$. The ratio of number-average particle length and thickness $\bar{l}_n/\bar{t}_n$ is generally larger than the ratio of the weight-average particle length and thickness $\bar{l}_w/\bar{t}_w$; however, the weight-average aspect ratio calculated from the values for individual particles, $\langle l/t\rangle_w$, is always larger than the corresponding number-average ratio, $\langle l/t\rangle_n$, as expected.

Figure 6 suggests how the clay particles evolve as the dispersion improves: large clay particles get smaller in both length and thickness, resulting in a higher particle density. Generally, as dispersion improves, there is a more rapid decrease in particle thickness than in particle length, resulting in an increase in particle aspect ratio. Figure 7a shows the decrease in number-average particle length ($\bar{l}_n$) and thickness ($\bar{t}_n$) as the degree of neutralization increases. Figure 7b shows the corresponding increase in particle density and the aspect ratios, $\langle l/t\rangle_n$ and $\bar{l}_n/\bar{t}_n$. The particle size continuously decreases with

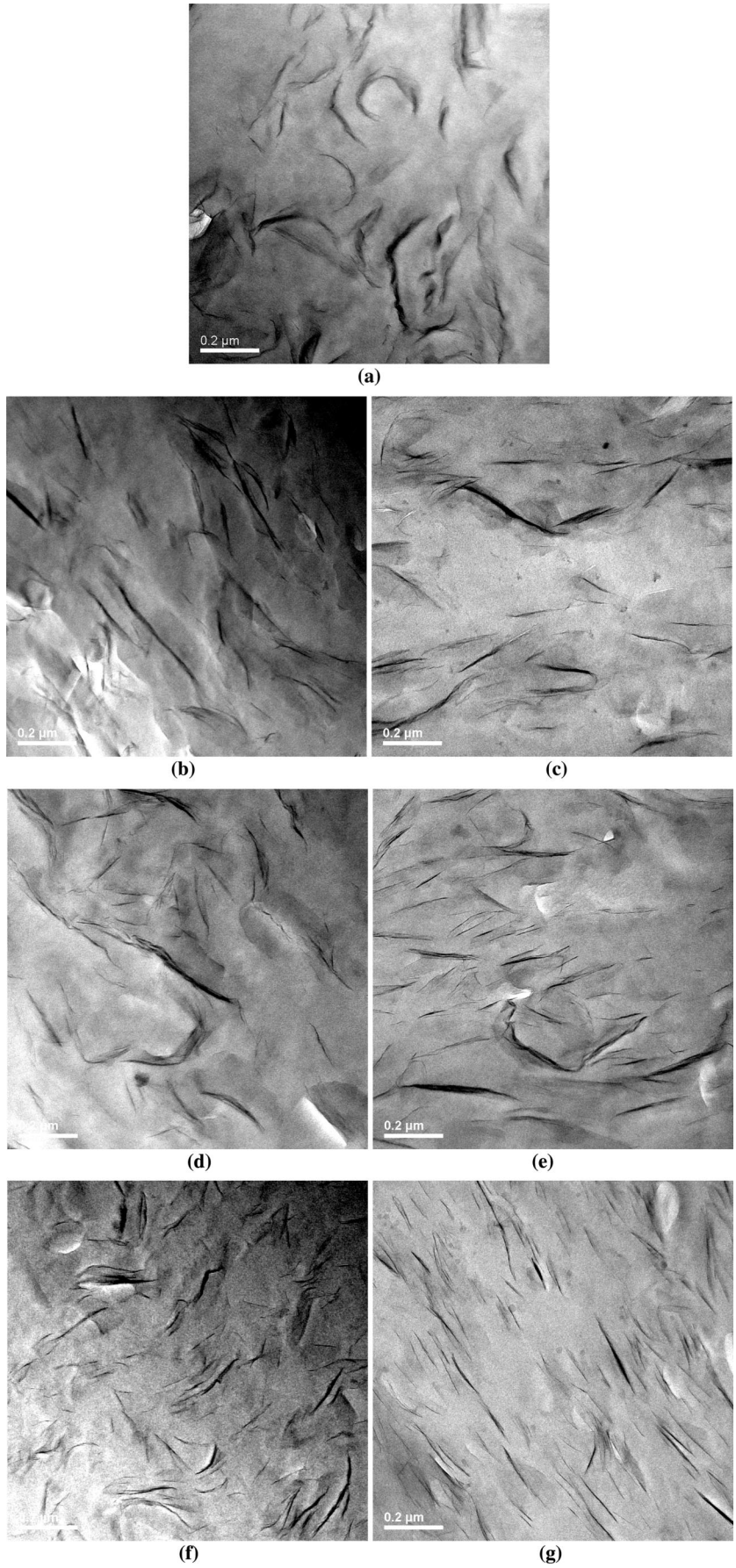

Figure 5. TEM micrographs of nanocomposites containing ~5 wt % MMT based on the $M_2(HT)_2$ organoclay and from EMAA copolymer and various sodium ionomers: (a) EMAA copolymer, (b) ionomer 1 (20% neutralized), (c) ionomer 2 (30% neutralized), (d) ionomer 3 (40% neutralized), (e) ionomer 4 (50% neutralized), (f) ionomer 5 (60% neutralized), and (g) ionomer 6 (70% neutralized).

Table 4. Results of Particle Analysis of Nanocomposites Based on the $M_2(HT)_2$ Organoclay (~5 wt % MMT)

polymer	neutralization level (%)	no. of particles analyzed	$\bar{l}_n$ (nm)	$\bar{t}_n$ (nm)	$\bar{l}_w$ (nm)	$\bar{t}_w$ (nm)	$\langle l/t \rangle_n$	$\bar{l}_n/\bar{t}_n$	$\langle l/t \rangle_w$	$\bar{l}_w/\bar{t}_w$
EMAA	0	580	231	11	300	23.3	28.1	20.6	34.9	12.9
ionomer 1	20	440	195	9.2	311	23.6	30.1	21.1	52.1	13.2
ionomer 2	30	534	189	8.8	287	28.4	30.4	21.4	53.4	10.1
ionomer 3	40	441	174	8.0	262	14.1	28.9	21.6	38.8	18.6
ionomer 4	50	517	160	6.9	230	12.7	32.1	23.0	62.9	18.2
ionomer 5	60	614	129	5.2	163	8.6	31.9	24.8	46.6	19.0
ionomer 6	70	667	126	3.8	167	6.2	44.2	33.4	73.1	26.7

increased degree of neutralization of the acid groups in terms of both particle length and thickness. Although aspect ratios do not change a lot with increased neutralization level, the particle density does increase progressively as the particle size decreases. From these results, it is clear that the organoclay exfoliation improves as the level of neutralization of acid groups increases.

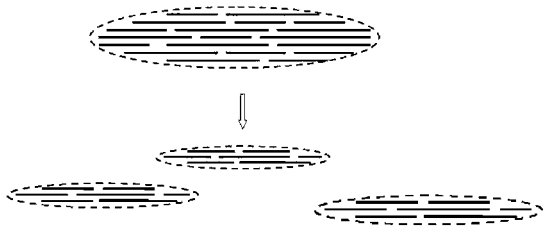

Figure 6. Schematic illustration of the evolution of clay particles during processing.

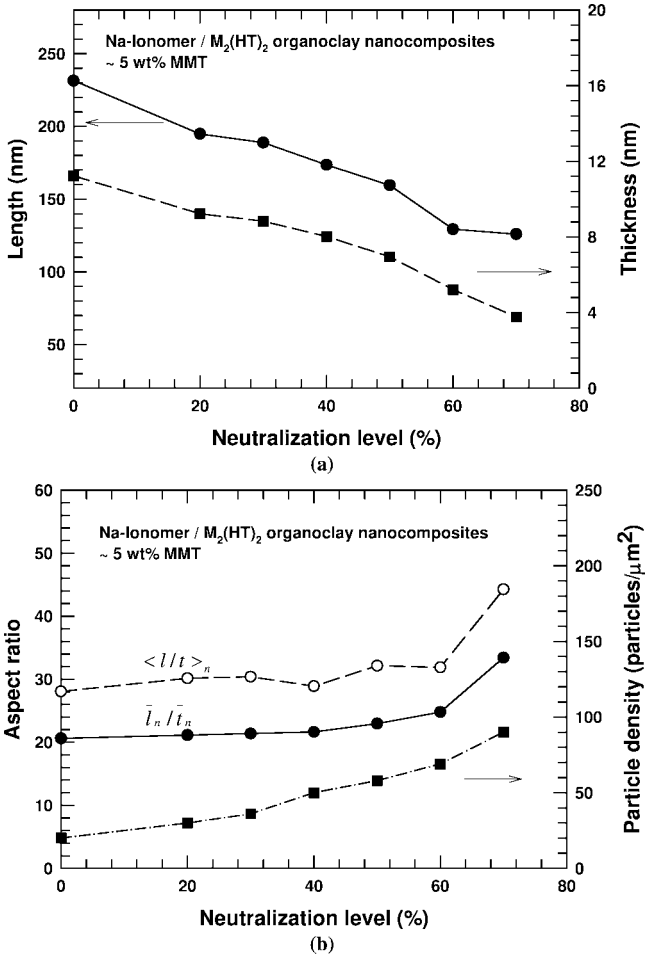

Figure 7. Effect of neutralization level on (a) particle length and thickness and (b) number-average particle aspect ratio and particle density for sodium ionomer nanocomposites at a fixed MMT content of ~5 wt %.

Mechanical Properties. Figure 8 shows representative stress−strain curves for nanocomposites prepared from the $M_2(HT)_2$ organoclay and ionomer matrices with various neutralization levels. As the neutralization level in the neat ionomer materials increases, the association among the ionic units becomes stronger and the volume of ionic aggregates increases, causing the modulus to increase and the elongation at break to decrease. The stress−strain diagrams of the neat ionomers with 30% and 50% neutralization reveal distinct yield points while the neat ionomer with 70% neutralization does not. For all the nanocomposites, no distinct yield point was observed. For each series of ionomer nanocomposites, the stress at most strain levels increases as the content of MMT increases.

The moduli of nanocomposites formed from the $M_2(HT)_2$ organoclay and ionomers with various neutralization levels are compared in Figure 9a as a function of their MMT content. As expected, the addition of the organoclay produces significant improvements in stiffness in all cases.

Since the moduli of the neat ionomers vary a great deal with neutralization level, it is useful to examine the relative moduli of the nanocomposites. Generally, the relative modulus reflects the level of organoclay exfoliation. However, the relative modulus is also a function of matrix modulus in addition to particle morphology, so caution must be exercised when making comparisons.[20,35] Figure 9b shows the relative moduli of nanocomposites with fixed clay loadings as a function of the neutralization level of the matrix polymers. For the same reason mentioned earlier, the data points for the acid copolymer are connected to those of the sodium ionomers by dashed lines. As shown by TEM and WAXS, the organoclay exfoliation improves as the neutralization level increases; however, the relative moduli data show an apparent minimum at about 40% neutralization. It is postulated that a combination of two effects lead to this trend. For nanocomposites with neutralization levels higher than 40%, the trend of better exfoliation with the elevated neutralization level leads to a greater reinforcing effect as one intuitively expects. The tensile moduli for the neat ionomers at these levels of neutralization (see Figure 3a) are relatively similar. On the other hand, at neutralization levels less than about 40%, the relative moduli decrease with increasing neutralization. Note that the tensile moduli of the neat matrix polymers in these ionomer nanocomposites are very low but are strong functions of the neutralization level. Composite theory shows that at a fixed filler level, for a given filler aspect ratio, low-modulus matrices lead to higher degree of reinforcement, i.e., E/E_m, than matrices with higher E_m; this effect is much more significant when the matrix polymer is very soft.[17,20,35,53,54] Thus, the decrease in E/E_m with increasing neutralization, at levels below about 40%, appears to stem from the relatively constant aspect ratio in this region (see Figure 7b) combined with the rapidly increasing E_m seen in Figure 3a.

Figure 10a compares the elongation at break for nanocomposites made from the EMAA copolymer and the six sodium ionomers as a function of their MMT content. Generally, as the clay content is increased, ductility decreases for most of the nanocomposites; however, for ionomer 5, which has half of its acid groups neutralized by sodium ions, the elongation at

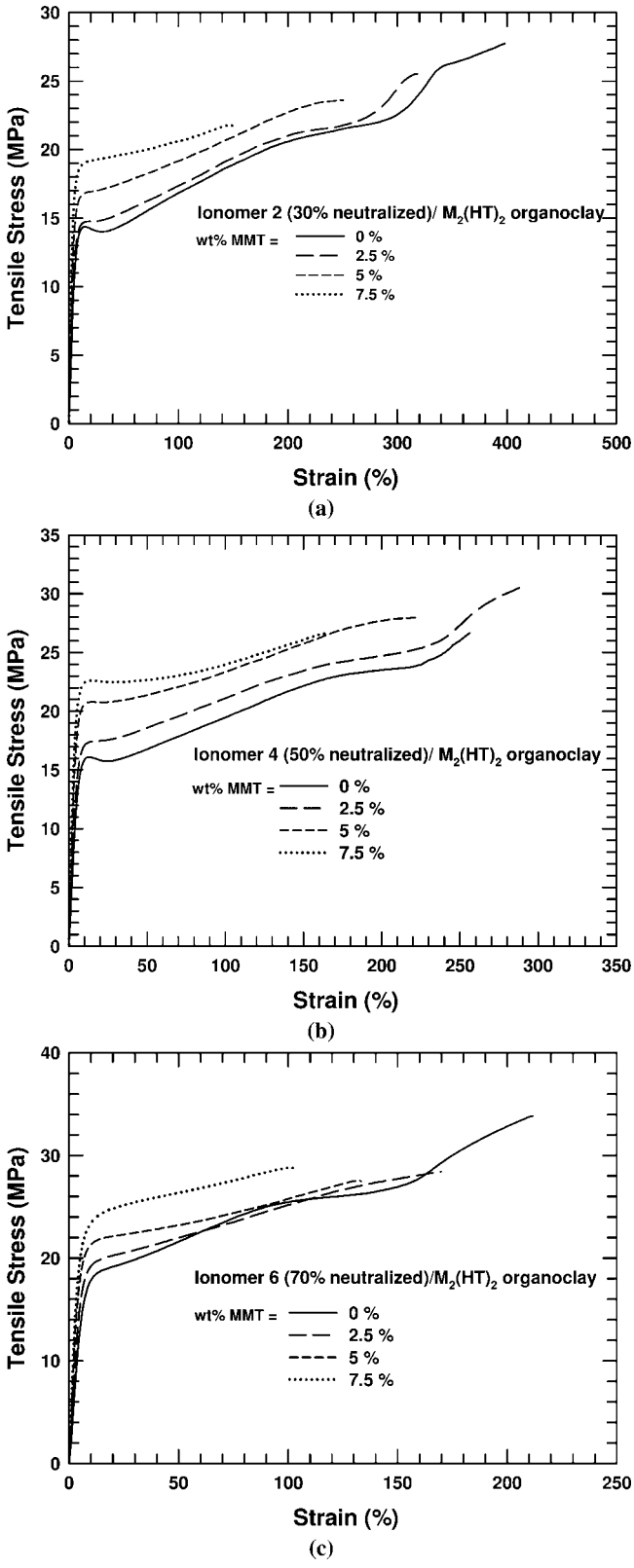

Figure 8. Stress−strain diagrams for nanocomposites based on the $M_2(HT)_2$ organoclay and various sodium ionomers: (a) ionomer 2 (30% neutralized), (b) ionomer 4 (50% neutralized), and (c) ionomer 6 (70% neutralized). The crosshead speed = 5.1 cm/min.

break first increases slightly with MMT loading, reaches a maximum at 2.5 wt % MMT, and then decreases as more montmorillonite is added. The elongation at break data are plotted versus neutralization level for fixed MMT contents in

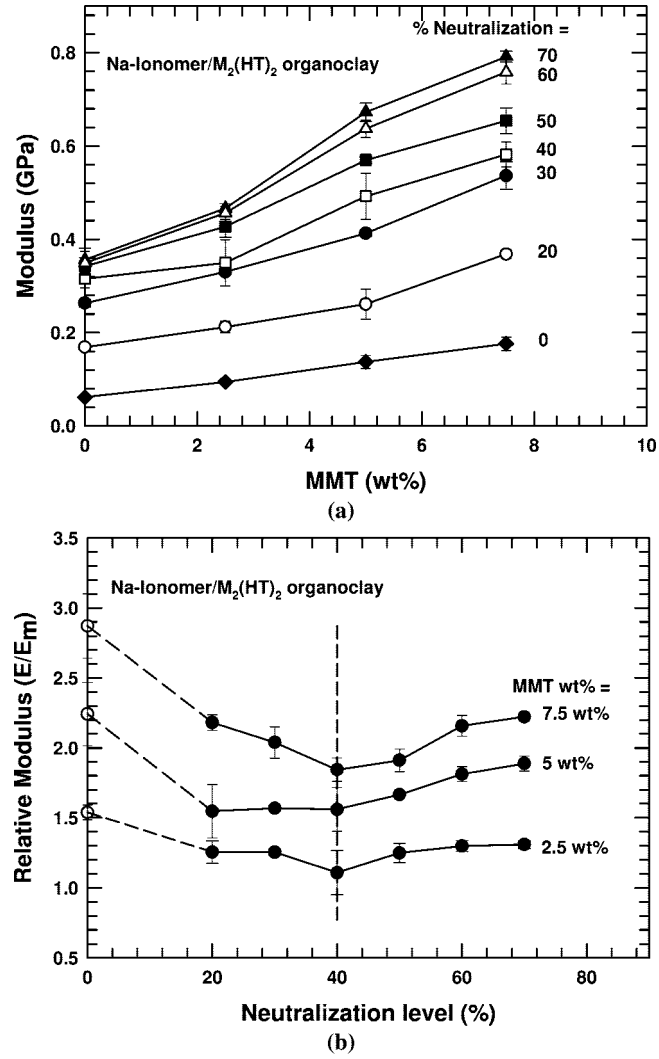

Figure 9. Modulus and relative modulus of nanocomposites formed from the $M_2(HT)_2$ organoclay and various sodium ionomers: (a) modulus as a function of montmorillonite content and (b) relative modulus as a function of neutralization level of ionomer matrices for nanocomposites with fixed MMT content.

Figure 10b. The data points for the acid copolymer are connected to those of the other sodium ionomers by dashed lines for the reason mentioned earlier. A trend of decreased ductility of nanocomposites as the clay content is increased can be clearly seen. However, the nanocomposites with a fixed MMT loading are simply mimicking the trend shown by the neat ionomers as the neutralization level changes.

Fracture toughness as judged by the Izod impact strength is an important property to be considered for some applications. Polymer nanocomposites based on polyolefins have been reported to have different impact values for the gate end and far end of injection-molded Izod bars.[29,30] Therefore, the impact strengths are averaged separately for the gate and far ends (see Figure 11). Generally, gate end samples show higher fracture energies than the far end samples; this could be a result of differences in platelet orientation between the two ends. Interestingly, instead of seeing a continuous loss of fracture energy with increasing MMT content, maximum values are observed for nanocomposites containing about 2.5 wt % MMT in most cases. After this maximum, addition of more clay leads to a decrease in the impact strength. These results are consistent with the previous reports from our laboratory.[25,55] It has been shown that the maximum at low clay concentration is due to

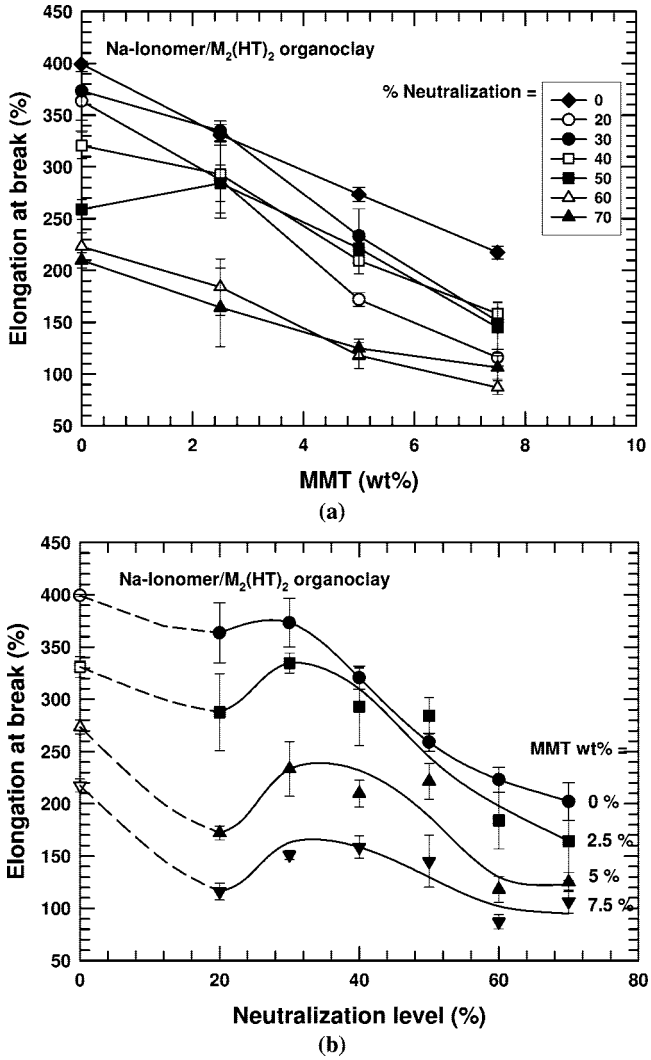

Figure 10. Elonation at break of nanocomposites formed from the $M_2(HT)_2$ organoclay and various sodium ionomers: (a) as a function of montmorillonite content and (b) as a function of neutralization level of ionomer matrices for nanocomposites with fixed MMT content.

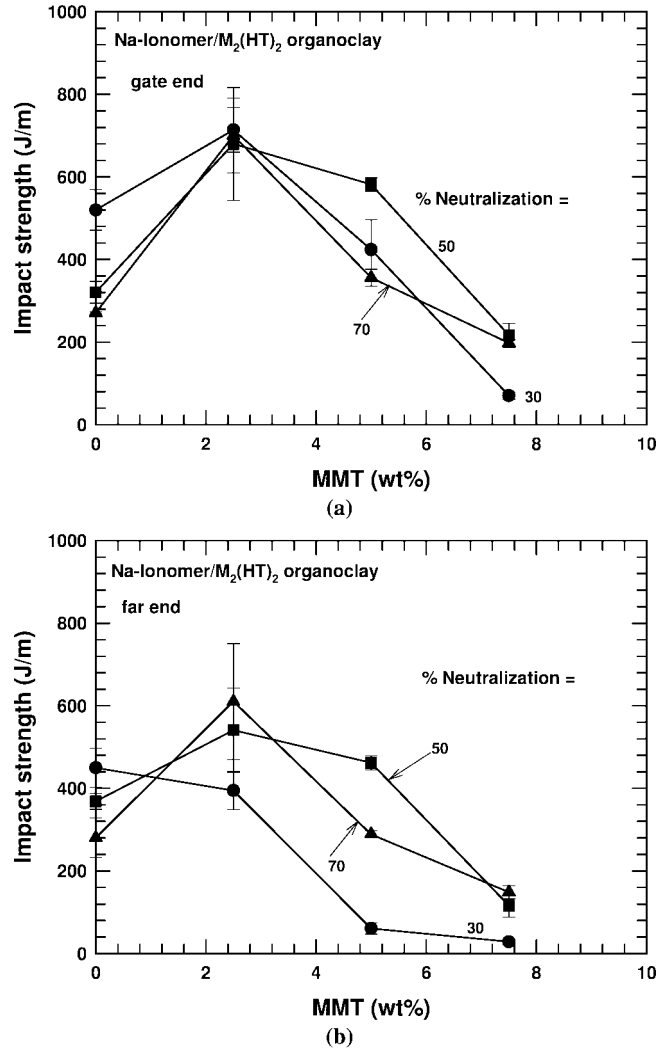

Figure 11. Impact strength of nanocomposites formed from the $M_2(HT)_2$ organoclay and various sodium ionomers as a function of montmorillonite content: (a) gate end and (b) far end.

the opposing effects of increased stiffness and yield strength vs reduced ductility.

Composite Model Predictions of Modulus. Theoretical modeling is an appealing approach for the design of polymer composite systems, and numerous models[53,56−58] have been proposed for predicting the properties of composites and for correlating experimental data with such predictions. One might question whether such theories can predict the behavior of composites based on nanosized fillers; however, previous papers[17,20,54,59] have shown this to be a useful approach.

The Halpin−Tsai equations are employed in this work to predict the tensile modulus of nanocomposites from the neat component properties and the particle aspect ratios as determined by quantitative particle analysis of TEM images. The expression for the longitudinal modulus[20,54,60] is

$$\frac{E^{(H-T)}}{E_m} = \frac{1 + 2(l/t)\phi_p\eta}{1 - \phi_p\eta} \tag{1}$$

where E_p and E_m are the modulus values of the filler particle and matrix polymer, respectively, ϕ_p is the volume fraction of the filler particles, (l/t) represents the filler aspect ratio, and η is given by

$$\eta = \frac{(E_p/E_m) - 1}{(E_p/E_m) + 2(l/t)} \tag{2}$$

In the model calculations, there are generally two ways of treating the filler particles. One is to boldly assume good exfoliation (method 1) with the MMT platelets themselves treated as the reinforcing filler particles. In this case, $E_p = E_{MMT} = 178$ GPa[54] and $\phi_p = \phi_{MMT} = 0.017$ at 5 wt % MMT.

Another way is to consider the partially exfoliated clay particles as parallel arrangements of MMT platelets and gallery material as described in previous reports[17,20,51,54,60,61] (method 2). The tensile modulus of such an effective particle can be estimated by using the following rule of mixtures

$$E_p = \nu_{MMT}E_{MMT} + \nu_{gallery}E_{gallery} \tag{3}$$

where ν_{MMT} and $\nu_{gallery}$ are the volume fraction of montmorillonite and the gallery space in the effective particle, while E_{MMT} and $E_{gallery}$ are their corresponding moduli. The volume fraction of MMT platelets, ν_{MMT}, is calculated as the ratio of the thickness of an individual platelet and the d-spacing of the nanocomposite as determined by the WAXS analysis

$$\nu_{MMT} = \frac{t_{platelet}}{d_{001}} \quad (4)$$

Considering that the modulus of the organic material in the gallery is significantly smaller than the modulus of the MMT platelets, eq 3 reduces to

$$E_p = \nu_{MMT} E_{MMT} \quad (5)$$

The volume fraction of the filler particles in the composites can be estimated as

$$\phi_p = \frac{\text{volume of MMT}}{\text{volume of nanocomposite}} \frac{\text{volume of filler particle}}{\text{volume of MMT}} = \frac{\phi_{MMT}}{\nu_{MMT}} \quad (6)$$

So in this case, the d_{001} values determined by WAXS are needed for the prediction using method 2. It is easy to determine the *d*-spacing from WAXS scans of nanocomposites based on matrices with low degrees of neutralization; however, at higher levels of neutralization, there are no distinctive peaks shown in the WAXS scans. Thus, there is no way to apply the partially exfoliated particle assumption for nanocomposites formed from ionomers with 40%−70% neutralization; only the tensile moduli of the nanocomposites formed from EMAA copolymer and sodium ionomers with 20% and 30% neutralization were predicted using this method. The parameters involved in the model calculations for these nanocomposites containing ~5 wt % MMT are listed in Table 5.

Figure 12 compares the experimental relative moduli of nanocomposites with those predicted by the Halpin−Tsai equations using both methods for composites prepared from the unneutralized acid copolymer and the sodium ionomers with 20% and 30% neutralizations; nanocomposites formed from ionomers with higher neutralization levels are not included due to the unavailability of estimates for d_{001}. The predictions using both methods are shown for a series of aspect ratios, 10, 20, 30, and 40, which span the range of the various experimental aspect ratios determined from the TEM images. Each prediction line shows a declining trend with the increase of neutralization level due to the increase in modulus of the matrix polymer; this quantitatively illustrates the previous argument that a given filler aspect ratio would produce more significant reinforcing effect in a softer matrix. It appears that predictions using method 1 fit the experimental data more closely, but it should be noted that this assumes the effective particles are single platelets which is obviously not realistic. On the other hand, the predictions by method 2, which assumes the intercalated structure of the effective particles and results in significantly increased volume fraction and decreased modulus of these effective filler particles, overestimate the moduli of these composites. These results actually suggest that the volume fraction of the filler particles has a more significant effect than does the modulus of the particles on the predicted moduli. The discrepancies between the experimental measurements and the Halpin−Tsai predictions are possibly due to the incomplete orientation of the clay platelets and the inadequate parameter estimations used, such as the volume fraction and modulus of the effective particles.[51]

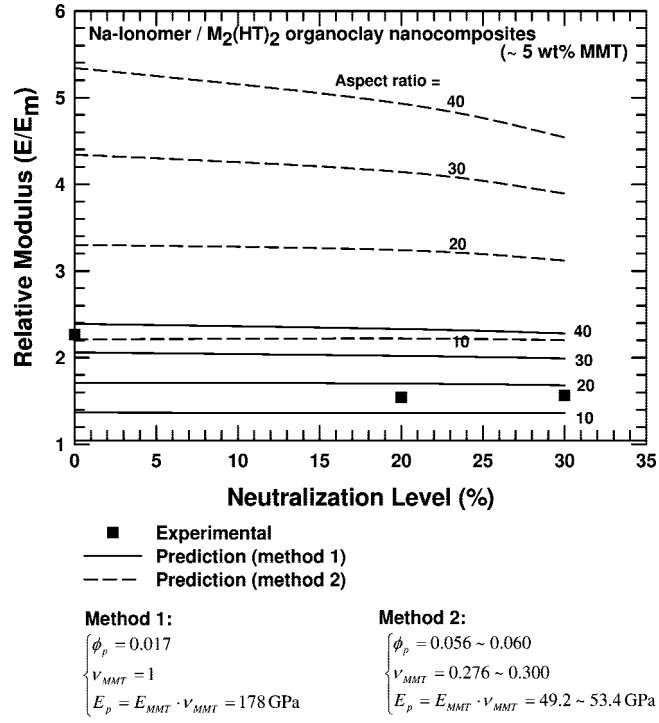

Figure 12. Comparison of experimental relative modulus of nanocomposites with predictions by the Halpin−Tsai model.

Conclusion

Morphology and mechanical properties of the EMAA-based ionomer nanocomposites are presented and discussed to obtain insights about the effect of the degree of neutralization of acid groups on the organoclay exfoliation. The nanocomposites formed were found to be rather well exfoliated but not to the extent found for polyamides. Clearly, the acid and ionic units in these polymers provide considerable beneficial effect for organoclay exfoliation compared to that can be realized in unmodified polyolefins.

An ethylene/metharylic acid copolymer and a series of sodium ionomers were melt mixed with the $M_2(HT)_2$ organoclay using a corotating twin-screw extruder to form nanocomposites. The differences in the rheology of these ionomers were partially compensated by varying the extrusion temperature according to the neutralization levels of these materials. TEM and WAXS results both reveal a mixed morphology of exfoliated structures and organoclay tactoids for all the nanocomposites formed. The exfoliation of the $M_2(HT)_2$ organoclay progressively improved as the neutralization level of the sodium ionomers was increased. The subsequent particle analyses quantitatively confirmed this conclusion by showing decreased particle length and thickness and increased particle aspect ratios and particle density with the increasing neutralization level. It seems that the ionic units on the polymer chain provide a more favorable interaction between the polymer matrix and the organoclay compared to acid units and, thus, lead to better dispersion of the clay particles. Mechanical properties were generally consistent with the morphology shown by TEM and WAXS. Better exfoliated nanocomposites usually show higher levels of reinforcement

Table 5. Parameters Used in the Halpin−Tsai Model (Method 2)

polymer matrix	organoclay	*d*-spacing (d_{001}, nm)	vol fraction of MMT in particle (ν_MMT)	modulus ;of particle (E_p, GPa)	modulus of the polymer matrix (E_m, MPa)	weight fraction of MMT in nanocomposites (%)	vol fraction of the filler in nanocomposites (ϕ_p)
EMAA	$M_2(HT)_2$	3.13	0.300	53.4	61	5	0.0556
ionomer 1	$M_2(HT)_2$	3.34	0.282	50.1	169	5	0.0590
ionomer 2	$M_2(HT)_2$	3.40	0.276	49.2	263	5	0.0601

and reduced elongation at break. The trends in relative moduli of the nanocomposites can be qualitatively explained by composite theory in terms of how neutralization level affects aspect ratio and the modulus of the ionomer matrix; however, the actual values calculated from the Halpin−Tsai equations do not quantitatively agree well with the experimental data. The discrepancies may be due to the incomplete orientation of the clay platelets and the inadequacy of the parameter estimations used.

Acknowledgment. The authors thank the E.I. DuPont Co., and Mark Wetzel in particular, for providing the polymers that made this investigation possible. We thank Southern Clay Products, Inc., for providing the organoclays and Mr. Tony Gonzalez for his help with WAXS analyses.

References and Notes

(1) Fornes, T. D.; Yoon, P. J.; Hunter, D. L.; Keskkula, H.; Paul, D. R. *Polymer* **2002**, *43* (22), 5915–5933.
(2) Giannelis, E. P. *Appl. Organomet. Chem.* **1998**, *12* (10/11), 675–680.
(3) Lee, H.-s.; Fasulo, P. D.; Rodgers, W. R.; Paul, D. R. *Polymer* **2005**, *46* (25), 11673–11689.
(4) Lee, H.-s.; Fasulo, P. D.; Rodgers, W. R.; Paul, D. R. *Polymer* **2006**, *47* (10), 3528–3539.
(5) Kim, D. H.; Fasulo, P. D.; Rodgers, W. R.; Paul, D. R. *Polymer* **2008**, *49* (10), 2492–2506.
(6) Bharadwaj, R. K. *Macromolecules* **2001**, *34* (26), 9189–9192.
(7) Messersmith, P. B.; Giannelis, E. P. *J. Polym. Sci., Polym. Chem.* **1995**, *33* (7), 1047–57.
(8) Yano, K.; Usuki, A.; Okada, A.; Kurauchi, T.; Kamigaito, O. *J. Polym. Sci., Polym. Chem.* **1993**, *31* (10), 2493–8.
(9) Gilman, J. W. *Appl. Clay Sci.* **1999**, *15* (1−2), 31–49.
(10) Gilman, J. W.; Kashiwagi, T.; Brown, J. E. T.; Lomakin, S.; Giannelis, E. P.; Manias, E. *Int. SAMPE Symp. Exhibit.* **1998**, *43* (Materials and Process Affordability--Keys to the Future, Book 1), 1053–1066.
(11) Bourbigot, S.; Le Bras, M.; Dabrowski, F.; Gilman, J. W.; Kashiwagi, T. *Fire Mater.* **2000**, *24* (4), 201–208.
(12) Varela, C.; Rosales, C.; Perera, R.; Matos, M.; Poirier, T.; Blunda, J.; Rojas, H. *Polym. Compos.* **2006**, *27* (4), 451–460.
(13) Lopez-Quintanilla, M. L.; Sanchez-Valdes, S.; Ramos de Valle, L. F.; Guedea Miranda, R. *Polym. Bull.* **2006**, *57* (3), 385–393.
(14) Galgali, G.; Ramesh, C.; Lele, A. *Macromolecules* **2001**, *34* (4), 852–858.
(15) Reichert, P.; Nitz, H.; Klinke, S.; Brandsch, R.; Thomann, R.; Mulhaupt, R. *Macromol. Mater. Eng.* **2000**, *275* (1), 8–17.
(16) Cui, L.; Paul, D. R. *Polymer* **2007**, *48* (6), 1632–1640.
(17) Cui, L.; Ma, X.; Paul, D. R. *Polymer* **2007**, *48* (21), 6325–6339.
(18) Li, X.; Ha, C.-S. *J. Appl. Polym. Sci.* **2003**, *87* (12), 1901–1909.
(19) Zanetti, M.; Camino, G.; Thomann, R.; Mulhaupt, R. *Polymer* **2001**, *42* (10), 4501–4507.
(20) Shah, R. K.; Kim, D. H.; Paul, D. R. *Polymer* **2007**, *48* (4), 1047–1057.
(21) Filippi, S.; Marazzato, C.; Magagnini, P.; Minkova, L.; Dintcheva, N. T.; Mantia, F. P. L. *Macromol. Mater. Eng.* **2006**, *291* (10), 1208–1225.
(22) Cerezo, F. T.; Preston, C. M. L.; Shanks, R. A. *Compos. Sci. Technol.* **2006**, *67* (1), 79–91.
(23) Huang, Y.; Ma, X.; Liang, G.; Wang, S.; Zhang, Q. *Polymer* **2008**, *49* (8), 2085–2094.
(24) Shah, R. K.; Paul, D. R. *Macromolecules* **2006**, *39* (9), 3327–3336.
(25) Shah, R. K.; Hunter, D. L.; Paul, D. R. *Polymer* **2005**, *46* (8), 2646–2662.
(26) Cui, L.; Khramov, D. M.; Bielawski, C. W.; Hunter, D. L.; Yoon, P. J.; Paul, D. R. *Polymer* **2008**, *49* (17), 3751–3761.
(27) Cui, L. Polymer-Organoclay Nanocomposites by Melt Processing. Ph.D. Dissertation, The University of Texas at Austin, **2009**.
(28) Fornes, T. D.; Paul, D. R. *Polim.: Cienc. Tecnol.* **2003**, *13* (4), 212–217.
(29) Shah, R. K.; Cui, L.; Williams, K. L.; Bauman, B.; Paul, D. R. *J. Appl. Polym. Sci.* **2006**, *102* (3), 2980–2989.
(30) Cui, L.; Hunter, D. L.; Yoon, P. J.; Paul, D. R. *Polymer* **2008**, *49* (17), 3762–3769.
(31) Stretz, H. A.; Paul, D. R.; Li, R.; Keskkula, H.; Cassidy, P. E. *Polymer* **2005**, *46* (8), 2621–2637.
(32) Hirasawa, E.; Yamamoto, Y.; Tadano, K.; Yano, S. *J. Appl. Polym. Sci.* **1991**, *42* (2), 351–362.
(33) Tachino, H.; Hara, H.; Hirasawa, E.; Kutsumizu, S.; Yano, S. *J. Appl. Polym. Sci.* **1995**, *55* (1), 131–138.
(34) Kutsumizu, S.; Tadano, K.; Matsuda, Y.; Goto, M.; Tachino, H.; Hara, H.; Hirasawa, E.; Tagawa, H.; Muroga, Y.; Yano, S. *Macromolecules* **2000**, *33* (24), 9044–9053.
(35) Fornes, T. D.; Paul, D. R. *Macromolecules* **2004**, *37* (20), 7698–7709.
(36) Fornes, T. D.; Yoon, P. J.; Keskkula, H.; Paul, D. R. *Polymer* **2001**, *42* (25), 09929−09940.
(37) Tierney, N. K.; Register, R. A. *Macromolecules* **2002**, *35* (6), 2358–2364.
(38) Tant, M. R.; Wilkes, G. L. Structure and properties of hydrocarbon-based ionomers. In *Ionomers: Synthesis, Structure, Properties and Applications*, 1st ed.; Tant, M. R., Mauritz, K. A., Wilkes, G. L., Eds.; Blackie Academic & Professional: London, 1997; pp 261−289.
(39) Bonott, S.; Bonner, E. F. *Macromolecules* **1968**, *1* (6), 510–515.
(40) Marx, C. L.; Cooper, S. L. *J. Macromol. Sci., Part B* **1974**, *B9*, 19.
(41) Goddard, R. J.; Grady, B. P.; Cooper, S. L. *Macromolecules* **1994**, *27* (7), 1710–1719.
(42) Kajiyama, T.; Oda, T.; Stein, R. S.; MacKnight, W. J. *Macromolecules* **1971**, *4* (2), 198–203.
(43) Tadano, K.; Hirasawa, E.; Yamamoto, H.; Yano, S. *Macromolecules* **1989**, *22* (1), 226–233.
(44) MacKnight, W. J.; McKenna, L. W.; Read, B. E. *J. Appl. Phys.* **1967**, *38* (11), 4208–4212.
(45) Grady, B. P. *Polym. Eng. Sci.* **2008**, *48* (6), 1029–1051.
(46) Longworth, R. Thermoplastic ionic polymers: ionomers. In *Ionic Polymers*; Holliday, L., Ed.; Applied Science Publishers: London, 1975; pp 69−172.
(47) Holliday, L. Classification and general properties of ionic polymers. In *Ionic Polymers*; Holliday, L., Ed.; Applied Science Publishers: London, 1975; pp 1−68.
(48) Kim, J. S.; Eisenberg, A. Ion aggregation and its effect on ionomer properties. In *Ionomers: Characterization, Theory, and Applications*; Schlick, S., Ed.; CRC Press: Boca Raton, FL, 1996; pp 7−34.
(49) Murali, R.; Eisenberg A. Glass Transition temperatures in styrene ionomers and their blends. In *Structure and Properties of Ionomers*; Pineri, M., Eisenberg, A., Eds.; Kluwer Academic Publishers: Dordrecht, 1986; pp 307−319.
(50) Chavarria, F.; Paul, D. R. *Polymer* **2006**, *47* (22), 7760–7773.
(51) Kim, D. H.; Fasulo, P. D.; Rodgers, W. R.; Paul, D. R. *Polymer* **2007**, *48* (18), 5308–5323.
(52) Kim, D. H.; Fasulo, P. D.; Rodgers, W. R.; Paul, D. R. *Polymer* **2007**, *48* (20), 5960–5978.
(53) Halpin, J. C.; Affdl, J. L. K. *Polym. Eng. Sci.* **1976**, *16* (5), 344–352.
(54) Fornes, T. D.; Paul, D. R. *Polymer* **2003**, *44* (17), 4993–5013.
(55) Yoo, Y.; Shah, R. K.; Paul, D. R. *Polymer* **2007**, *48* (16), 4867–4873.
(56) Halpin, J. *J. Compos. Mater.* **1969**, *3* (4), 732–734.
(57) Hill, R. *J. Mech. Phys. Solids* **1965**, *13* (4), 213–222.
(58) Hill, R. *Proc. Phys. Soc., London* **1952**, *65A*, 349–54.
(59) Chavarria, F.; Paul, D. R. *Polymer* **2004**, *45* (25), 8501–8515.
(60) Sheng, N.; Boyce, M. C.; Parks, D. M.; Rutledge, G. C.; Abes, J. I.; Cohen, R. E. *Polymer* **2004**, *45* (2), 487–506.
(61) Brune, D. A.; Bicerano, J. *Polymer* **2002**, *43* (2), 369–387.

MA900105W